Biodivers Conserv (2015) 24:841–863
DOI 10.1007/s10531-015-0907-7

ORIGINAL PAPER

Microstructure and cyanobacterial composition of microbial mats from the High Arctic

Asunción de los Ríos[1] · Carmen Ascaso[1] · Jacek Wierzchos[1] · Warwick F. Vincent[2] · Antonio Quesada[3]

Received: 4 December 2014 / Revised: 16 February 2015 / Accepted: 4 March 2015 /
Published online: 10 March 2015

Abstract Arctic lakes, ponds and streams contain benthic microbial mats that are dominated by cyanobacteria, and these communities often account for a large proportion of the total ecosystem biomass and productivity. The vertical structure and composition of mats from two different aquatic habitats in the Canadian High Arctic, Ward Hunt Lake and a polar desert stream were analyzed in detail by microscopy techniques. Two distinct layers were identified in each mat: a surface layer with a high density of cells and associated extracellular polymeric substances (EPS), and a less cohesive bottom layer with an accumulation of mineral particles. The matrix formed by the cyanobacterial filaments and EPS produced the complex microstructure of all three mats, and likely favoured different microenvironments where specialized microbial interactions and biomineralization processes could take place. Structural and compositional differences were found among the mats. The lake mat had a surface layer of *Dichothrix*, and contained abundant particles of calcium carbonate, while *Tychonema*-like and *Tolypothrix*-like appeared mainly in the stream mats, along with a higher diversity of Chroococcales. A black microbial mat from one of the stream sites had markedly lower diversity than the other mat types. The observed differences in cyanobacterial composition and physical structure may be related to habitat stability and the availability of liquid water.

Keywords Cyanobacteria · Habitat stability · Microbial ecology · Polar regions · Water availability

Communicated by Anurag chaurasia.

✉ Asunción de los Ríos
arios@mncn.csic.es

[1] Museo Nacional de Ciencias Naturales, CSIC, Serrano 115 dpdo, 28006 Madrid, Madrid, Spain

[2] Centre d'études nordiques (CEN) & Dépt de Biologie, Université Laval, Quebec City, QC G1V 0A6, Canada

[3] Dpt. Biología, Universidad Autónoma de Madrid, 28049 Madrid, Spain

Introduction

Freshwater ecosystems in the polar zones are subjected to extreme environmental conditions including large variations in light availability and temperature, in combination with periods of freezing and a short season of open water conditions (Villeneuve et al. 2001). Cyanobacterial communities often dominate Arctic and Antarctic freshwater ecosystems, particularly the benthic habitats of lakes, ponds and streams where microbial mats form highly pigmented biofilms that carpet the bottom substrata (Singh and Elster 2007; Quesada and Vincent 2012; Vincent and Quesada 2012). Microbial mat communities growing in surface melt pools on ice polar regions are dominated by oscillatorian cyanobacteria (Vincent et al. 2000; De los Ríos et al. 2004), although other cyanobacterial groups, notably in the orders Nostocales and Chroococcales are also present and are abundant (Jungblut et al. 2005; Jungblut et al. 2010; Taton et al. 2008; Verleyen et al. 2010; Lionard et al. 2012). All of these cyanobacterial taxa are known to secrete mucilaginous organic compounds and bind together sediment particles, resulting in cohesive mats and films that offer protected microhabitats for less tolerant biota, algae, heterotrophic protists and microinvertebrates (Vincent et al. 2000). An enormous diversity of heterotrophic bacteria is also known to occur within such mats (Varin et al. 2010). Cyanobacteria are thus not only the main primary producers in these systems, but they also provide organic substrates and the physical scaffolding for the many other components of the microbial mat consortia (Noffke et al. 2003; De los Ríos et al. 2004).

Photosynthetically active radiation (PAR) is strongly attenuated through the vertical profile of polar microbial mats (Quesada et al. 1999), and this provides sharp gradients of redox and other biogeochemical properties, from oxygen supersaturation at the surface to anoxic conditions at the bottom, where anaerobic processes take place (Fernández-Valiente et al. 2007). These gradients promote the growth of the different elements of the mat microbial community with different ecological roles (Paerl and Pinckney 1996). Some organisms in the microbial mat can adjust their position within the mat profile to their optimal environmental conditions (e.g. radiation, redox potential, etc.; Quesada et al. 2001). The chemical characteristics of the interstitial water within the mat are known to be different to those of the overlying water column (Vincent and Quesada 2012; Villeneuve et al. 2001). However, the chemistry of the ambient water can also have a strong influence on the formation of these biogeochemical gradients within the mats (Petroff et al. 2010).

The three dimensional microstructure of microbial mats is best investigated with a combination of different, complementary microscopic techniques such as optical, scanning electron and confocal scanning laser microscopies. For example, the combined application of these approaches to microbial mats on the McMurdo Ice Shelf (Antarctica) revealed a pronounced vertical stratification of cyanobacterial taxa and mineral sediments, a high content of extracellular polymeric substances (EPS), and large void spaces within the matrix that were occupied by water (De los Ríos et al. 2004).

In spite of the major importance of freshwater microbial mats in the High Arctic, they have been investigated only recently from a structural perspective (e.g., Lionard et al. 2012). In this paper we extend the knowledge of these mat communities in the Arctic, with attention to the variability among mat types. We sampled mats from three contrasting sites, a lake and two streams, located in the northern Ellesmere Island region of the Canadian High Arctic. We then applied a range of microscopy techniques to examine mat microstructure and cyanobacterial composition. As the purpose of this article is not taxonomical, we have not included species names and even the generic names should not be consider of taxonomical value but rather as morphological approximations.

Materials and methods

Study sites and sample collection

In the Arctic summer of 2000–2001, microbial mats from two freshwater ecosystems were sampled in the northern Ellesmere Island region, Canadian High Arctic: Ward Hunt Lake (Fig. 1a) on Ward Hunt Island (83°02′N, 73°15′W), and a stream at Taconite Inlet (Fig. 1b), on the northern coast Ellesmere Island (82°50′N, 78°00′W). These waters occur in polar desert catchments with sparse vegetation. Ward Hunt Lake is a small waterbody (area = 0.35 km^2; Zmax = 10 m) with perennial ice cover over most of its surface but a moat section on its western side that thaws every summer. The water temperature during the study period ranged between 1 and 9 °C over the 24 h cycle, conductivity was 140 µS cm^{-1} and pH 8.38, with 100 % oxygen saturation (13.35 mg/L at 1.3 °C). The stream investigated (designated stream C1) collects water from melting snowbanks from the hills close to Lake C1 and has a 4 m wide but shallow (10–20 cm deep) flowing water

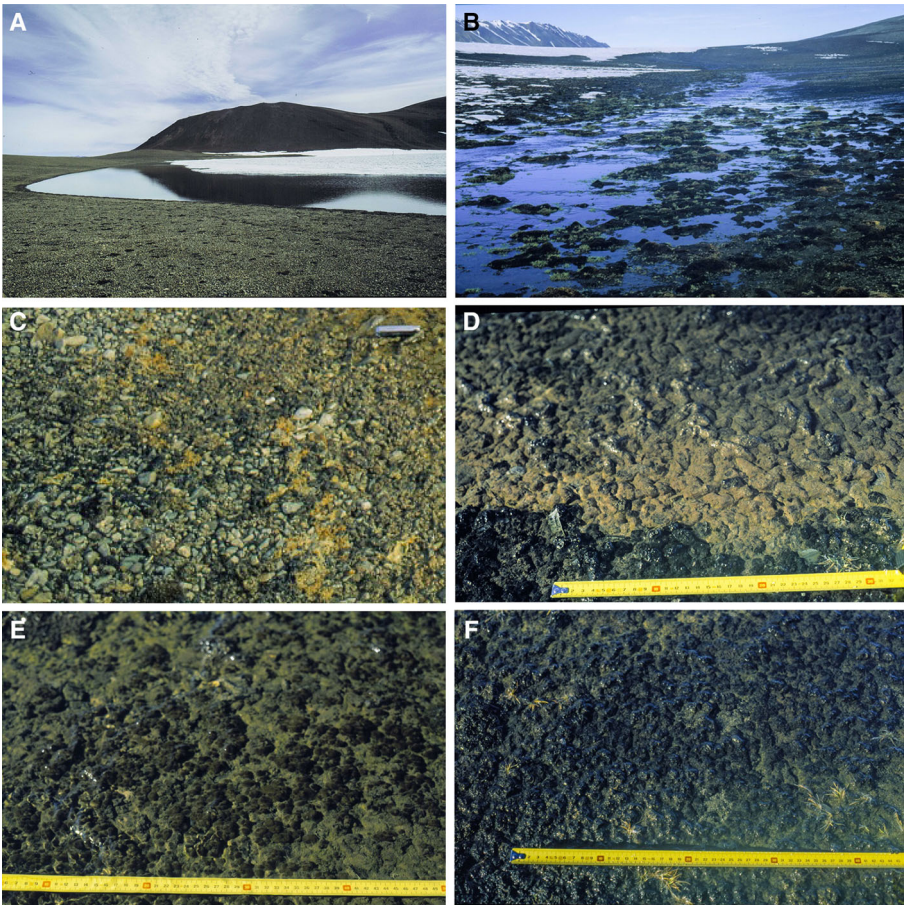

Fig. 1 **a** Ward Hunt lake. **b** Stream C1 at Taconite Inlet. **c** View of the surface of Ward Hund lake mat. **d** View of the surface of Stream C1, showing *pink* and *black* microbial mats. **e** View of the surface of *pink* mat in stream C1. **f** View of the surface of *black* mat in stream C1

layer with temperatures ranging from 4 to 12 °C. Its conductivity was 197 μS scm^{-1}, pH was 7.21, and the oxygen was at 100 % saturation. Chemical analyses (Table 1) indicated similar conditions at the two sites, with oligotrophic, low nutrient and major ion concentrations. Nutrient concentrations in Ward Hunt Lake were somewhat lower than in the stream.

The microbial mats were collected by cutting squares of 5 by 5 cm of the cohesive layer and placing them on a plastic tray using an alcohol-sterilized plastic spatula. Several cores of this mat were then subsampled with a metal corer of 11 mm inner diameter. In Ward Hunt Lake, the microbial mats carpeted the bottom of most of the eastern shallow water littoral zone (Fig. 1c), and samples were near the shore from 10 to 15 cm depth. Stream C1 in Taconite Inlet showed two morphologically distinct mats that also differed in color and distribution (Fig. 1d). Pink colored mats occurred in 5–10 cm depth of flowing water (Fig. 1e), while black mats (Fig. 1f) occurred on raised sections of the stream bed where the substrate was saturated but not completely immersed in flowing water at the time of collection. The mat samples for microscopy were transferred immediately to tubes containing 3 % glutaraldehyde in a phosphate buffer (100 mM; pH 7.1). The samples were fixed for 3 h, washed twice with phosphate buffer (100 mM; pH 7.1) and then stored at 4 °C until further analysis. The remaining mat samples were placed on dry absorbent paper for 30 s to remove the excess water and stored in sterile plastic bags at −80 °C until further analysis. Subsamples were also observed immediately in the field by light microscopy.

Optical microscopy

The frozen samples were placed in sterile petri dishes and after thawing at room temperature were observed intact under a Leica MZ12.5 stereoscope at 5–50× magnification. The mats were then teased out with forceps and further examined. Different sections of the mats were separated with a scalpel blade, placed on slides and observed at 40–1000× with an Olympus BH10 fluorescence microscope equipped with a DFC 300EFX Leica camera. Five core samples from each mat type were analyzed in this way.

Confocal laser scanning microscopy (CLSM), scanning electron microscopy (SEM) and X-ray energy dispersive spectroscopy (EDS)

The samples for CSLM, SEM and EDS were prepared according to the procedures described in De los Ríos et al. (2004). In brief, the in situ glutaraldehyde fixed samples (see above), were then fixed in the laboratory with osmium tetroxide (with the exception of the samples for CSLM), dehydrated in a series of ethanol solutions, and embedded in LR-White resin. Blocks of resin-embedded mats samples were finely polished.

CSLM samples were examined with LSM 310 Zeiss confocal microscope. An argon laser was used to generate an excitation wavelength of 488 nm and the resultant emission

Table 1 Water chemistry of C1 stream (C1-S) and Ward Hunt Lake (WHL)

Site	DOC	DIC	SRP	NO_2–N	NO_3–N	TN	TP	SiO_2	Ca
C1-S	1.3	19.8	0.021	0.003	0.038	0.156	nd	nd	nd
WHL	0.3	1.8	0.005	0.001	0.018	0.059	0.004	0.07	5.57

Values are in mg l^{-1}

nd non determined

was filtered through a long pass filter (>515 nm). The three-dimensional images were made up of several confocal sections at 0.5–1 μm increments through the sample, by computer assisted microscopy, and three-dimensional reconstruction was then applied to visualize the mat microstructure.

Osmium tetroxide fixed samples were carbon coated and examined using DSM-960 Zeiss and FEI INSPECT SEM microscopes, both equipped with a four-diode, semiconductor BSE detector and a Link ISIS microanalytical EDS system. The samples were studied in Back Scattered electron mode (SEM–BSE). EDS examination of the samples was simultaneously performed. The microscope was operated at 15 kV acceleration potential and 1–5 nA specimen current.

Low temperature scanning electron microscopy (LTSEM)

Small microbial mat fragments were sprayed with distilled water and, after eliminating excess water, were mechanically fixed onto the specimen holder of a cryotransfer system (Oxford CT1500), immediately cryofixed by plunging into subcooled liquid nitrogen, and then transferred to the microscope preparation unit via an air-lock transfer device following the protocol described in (De los Ríos et al. 2004). The frozen specimens were cryofractured in the preparation unit and transferred directly via a second air lock to the microscope cold stage where they were etched for 2 min at −90 °C. After ice sublimation, the etched surfaces were gold sputter-coated in the preparation unit and the specimens placed on the cold stage of the SEM chamber. Fractured surfaces were observed using a Zeiss DSM-960 SEM microscope at −135 °C.

Morphological identification of cyanobacteria

Five cores from each microbial mat were observed under the optical microscope to identify the different morphologies. The identification of the different cyanobacteria was done to genus level following Komarek and Anagnostidis (1989, 1999, 2005). The morphological characteristics of the different taxa were recorded in detail, including cell size and the cellular arrangement in colonies. A total of 100 cells of each morphotype were measured and the average was calculated. If the average length and breadth of the different morphologies fell within the range of 1 standard deviation of the mean, the taxa were considered morphologically identical. No taxonomical identification was intended in this work.

Results

Biological description

The microbial mats were dominated by cyanobacteria, with associated microalgae belonging to different taxonomic groups, diverse mineral agglomerates and large amounts of extracellular polymeric substances (EPS). Bacteria, fungi and metazoans were also present, but were not identified. There were differences in microstructure as well as in phototrophic composition and the quantity of mineral particles.

Ward Hunt Lake mat

Macroscopically, this mat was 3–5 mm thick with a pink-orange surface embedded with numerous dark gelatinous colonies. There were two distinct layers, as visualized by LTSEM (Fig. 2), that could be readily separated. The thin surface layer (noted by arrows in Fig. 2) had a more cohesive structure than the looser thick bottom layer that was dark

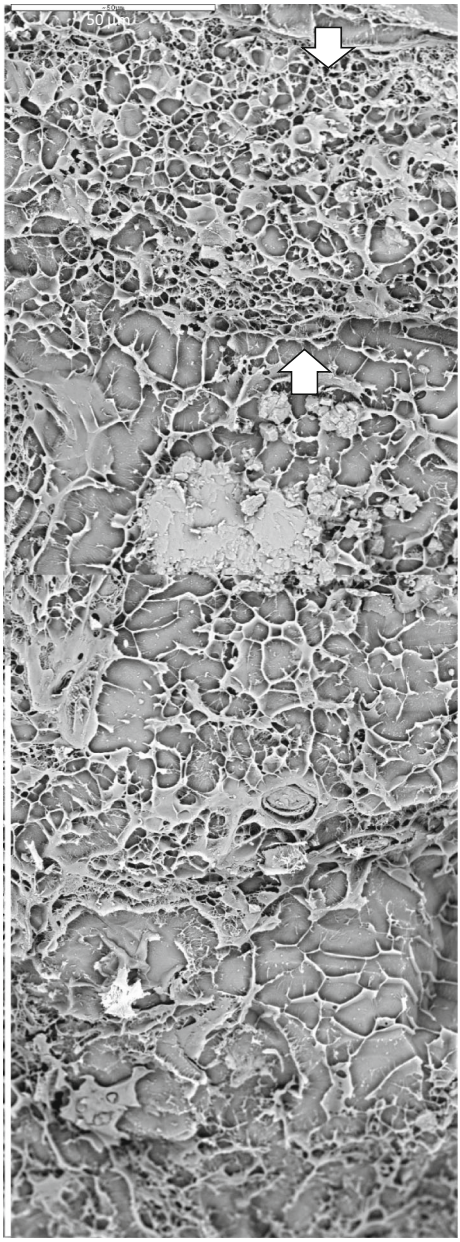

Fig. 2 General view of Ward Hunt Lake mat (LTSEM). *Arrows* point to the upper layer of the mat

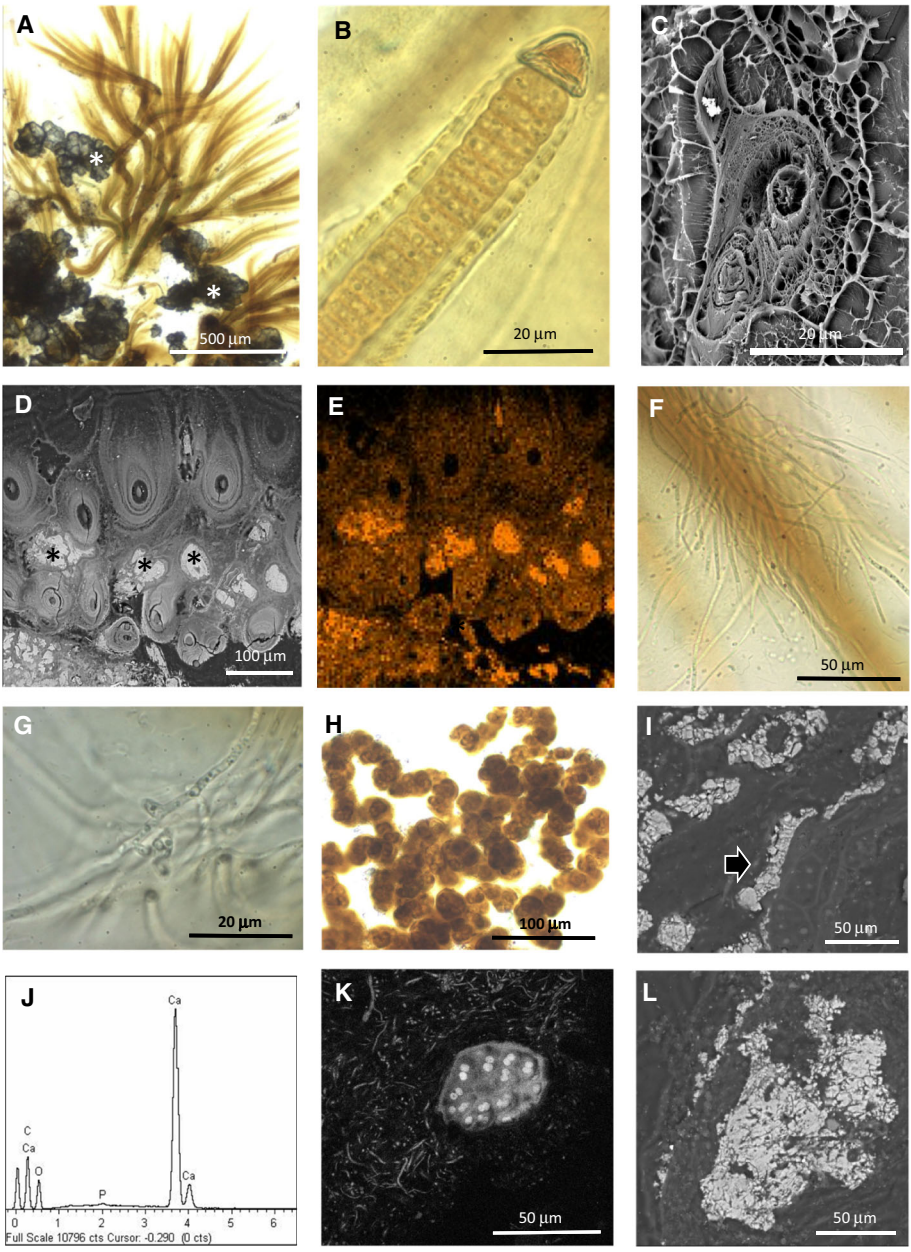

Fig. 3 Upper layer of Ward Hunt Lake mat. **a** Optical image of *Dichothrix* sp. colony at the surface of the mat and associated mineral particles (*asterisks*). **b** Optical image of *Dichothrix* sp. filament. **c** LTSEM image of transversely sectioned terminal zones of *Dichothrix* sp. filaments. **d** SEM–BSE image of *Dichothrix* sp. layer showing association with calcium carbonate particles (*asterisks*). **e** EDS map of calcium in the area of (**d**). **f** Optical image of thin filamentous cyanobacteria surrounding a *Dichothrix* filament. **g** Optical image of fungi present in (**e**) area. **h** Optical image of *Nostoc* colony. I, SEM–BSE image of *Nostoc* cells associated with calcium carbonate deposits (*arrow*). **j** Spectrum of the mineral deposit indicated by an *arrow* in (**i**). **k** CSLM image of *Nostoc* colony immersed in the thin filamentous cyanobacterial matrix. **l** SEM–BSE image of calcium carbonate deposits present in the thin filamentous cyanobacterial matrix

green in colour. The bottom contained abundant populations of thin oscillatorian cyanobacteria and it fluoresced more intensively under the fluorescence microscope with green excitation than the surface layer.

The surface, near-spherical dark gelatinous colonies were composed of *Dichothrix* sp. (Fig. 3a, b), with inclusions of mineral particles (asterisks). The largest observed cell (close to the heterocyst) was 18.0 μm wide and 3.7 μm long, while the heterocyst in this

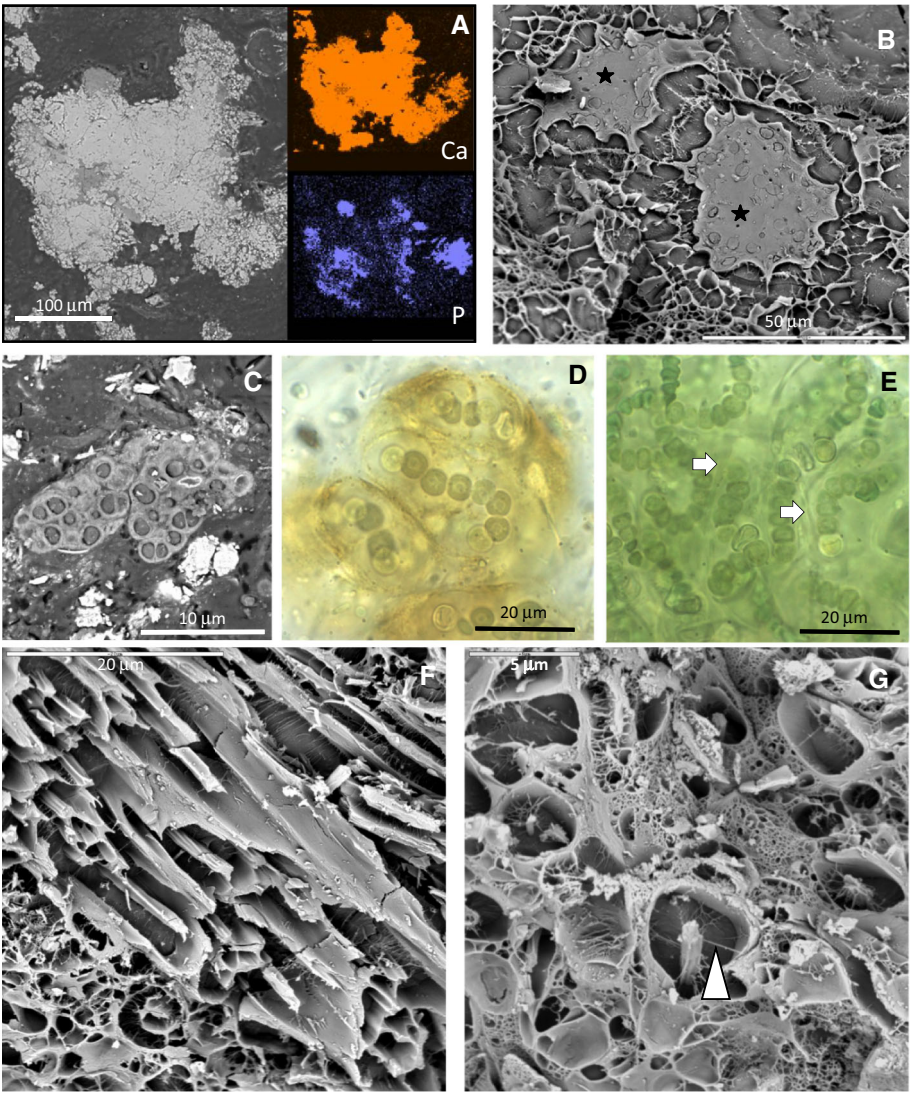

Fig. 4 Bottom layer of Ward Hunt lake mat. **a** SEM–BSE image and EDS map of calcium and phosphorus of one of the mineral particles present in this layer. **b** LTSEM image of cyanobacterial microcolonies with dense mucilage (*stars*). **c** SEM–BSE image of *Chroococcus*-type colony. **d** Optical image of *Nostoc* colony with almost spherical cells. **e** Optical image of *Nostoc* colony with cylindrical cells. *Arrows* note thin cyanobacterial filaments. F, LTSEM image of thin cyanobacterial trichomes of striate cell walls. **h** LTSEM image of a transversely sectioned trichomes showing EPS fibers connecting the cell (*arrow*) with external envelope

filament was 20.2 by 13.4 μm. The heterocysts averaged 8.8 by 4.4 μm, and the largest cells in each filament averaged 12.2 by 3.8 μm. In some cases the *Dichothrix* sheaths were empty. The outer terminal zone of the filaments had a broad envelope of different layers of EPS, which created a denser matrix around the cells (Fig. 3c). These envelopes had associated deposits of $CaCO_3$, as visualized by SEM–BSE (asterisks in Fig. 3d) and EDS (clear spots in the Ca distribution map, Fig. 3e). The *Dichothrix* filaments were surrounded by thin filamentous cyanobacteria (cf. *Leptolyngbya*; Fig. 3f) that fluoresced red on a fluorescence microscope using green excitation. Fungal-like hyphae were also observed surrounding the filament sheaths (Fig. 3g). There were additionally small flattened colonies at the surface that were black and also contained mineral particles. Light microscopy revealed that these were *Nostoc* colonies, with short filaments only a few cells long, embedded within dense orange sheaths (Fig. 3h). The cells were 5.9 by 7.6 μm and heterocysts 5.0 by 3.7 μm. Calcium carbonate deposits were observed associated with these cells, as revealed by SEM–BSE microscopy (Fig. 3i) and spot qualitative EDS microanalysis (Fig. 3j). These colonies were solidly attached to the mat, which was composed of a matrix of thin filamentous cyanobacteria of several sizes and shapes (Fig. 3k), containing numerous calcium carbonate particles (Fig. 3l). At the interphase between the two layers, there were two sizes of oscillatorians: filaments of ca. 4 μm diameter that fluoresced red on fluorescence microscope and thinner filaments of around 2.5 μm diameter that fluoresced orange, implying higher concentrations of phycoerythrin in the latter.

The bottom layer of the Ward Hunt mats contained higher concentrations of thin oscillatoriales, with the presence of mineral particles (Fig. 2). EDS microanalysis showed that these particles were composed mostly of calcium carbonate (Fig. 4a). Empty *Dichothrix* sheaths were also found at the bottom layer, along with microcolonies of the genera *Nostoc*, cf. *Gloeocapsa* and cf. *Chroococcus* (Fig. 4b, c). Two distinct morphologies of *Nostoc* colonies were identified in this bottom layer, one with almost spherical cells (3.8 × 3.7 μm, with heterocysts 4.7 × 4.8 μm; Fig. 4d), and the other with a yellow sheath and cylindrical cells (4.2 × 2.6 μm, with heterocysts 4.9 × 4.2 μm; Fig. 4e). Thin cyanobacterial filaments were intermixed with *Nostoc* cells within the colonies (arrows in Fig. 4e). The *Gloeocapsa*-type and *Chroococcus*-type colonies (Fig. 4c) were composed of groups of cells with lamellar, well delimited mucilaginous sheaths. Flat filaments of cyanobacteria with widened and lamellated sheath (likely *Tolypothrix*) were also observed in transition zone of the mat, and thin cyanobacterial trichomes with striate cell walls were also abundant (Fig. 4f). These latter filaments were observed by LTSEM with similar orientations and within wide cavities in the mat (Fig. 4g). Some radial EPS fibres connecting the cells with the external envelope were the only component observed in the cavities (arrowhead in Fig. 4g). The thin oscillatorians in the matrix were diverse in size and morphology (Fig. 5a), including false-branching cf. *Plectonema* of two different diameters (arrow in Fig. 5a, b), *Pseudanabaena*-type (Fig. 5c), and *Leptolyngbya*-type with different diameters (Fig. 5d, e). Wider oscillatorians were also found, with four different diameters: 2, 4.6, 7 and 10 μm (Fig. 5f–h). Broader green algal filaments including cf. *Zygnema* (20 × 21 μm), and many diatom taxa were also found (Fig. 5g).

Pink mat in stream C1

Macroscopically, the immersed stream mat was 3–4 mm in thickness and was composed of two layers (Fig. 6). The surface layer was pink-orange in colour, and inlaid with black colonies. This overlaid bottom layer was intense green in colour. The two layers were well

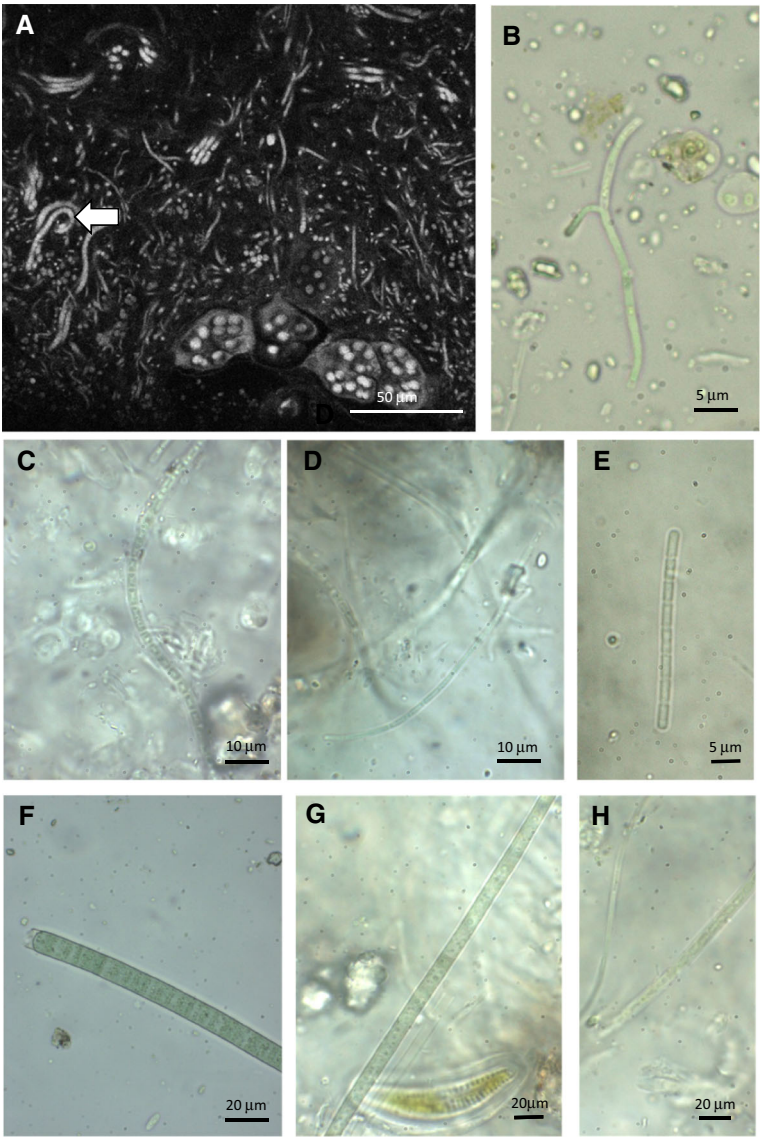

Fig. 5 Bottom layer of Ward Hunt Lake mat. **a** CSLM image of the matrix formed by thin oscillatoriales. *Arrow* notes *Plectonema*-type filaments. **b–h** Optical images of false-branching cf. *Plectonema* (**b**), cf. *Pseudanabaena* (**c**), cf. *Leptolyngbya* (**d, e**) and wide oscillatoriales (**f, h**) filaments

connected and could only be separated by scalpel. The surface layer contained diverse morphotypes of filamentous and colonial cyanobacteria. It was non-fluorescent under green excitation on fluorescence microscope, despite the presence of thick filamentous cyanobacteria. The bottom layer was highly fluorescent under green excitation, due to a high abundance of thin filamentous cyanobacteria in combination with thick filaments and microcolonies. LTSEM showed considerable variations in microstructure depending on the density of cells and EPS (Fig. 6). The upper part of the mat (noted by arrows in Fig. 6) was

Fig. 6 General view of *pink* mat in stream C1 (LTSEM). *Arrows* note the upper layer of the mat

a compact layer with the agglutination of cells by a large amount of EPS (Fig. 7a), while the bottom layer was formed by dispersed cyanobacterial cells or trichomes (Fig. 6). In addition to cyanobacteria, diatoms (Fig. 7b) and green algae were also commonly observed. These algal cells were fully immersed in the EPS matrix, which also contained fungal-like hyphae (white arrows in Fig. 7b) and bacterial cells (black arrows in Fig. 7b).

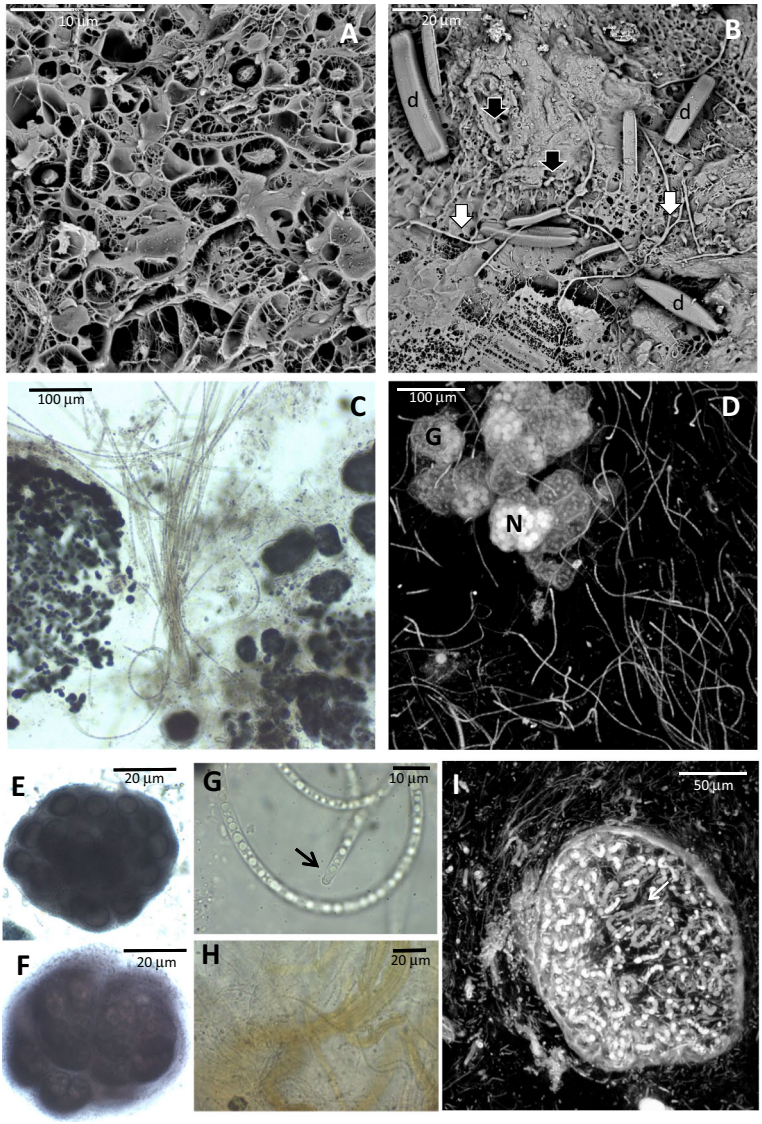

Fig. 7 Upper layer of *pink* mat in stream C1. **a** LTSEM image of the upper layer. **b** LTSEM image of diatoms (**d**) embedded in the EPS matrix containing fungal (*white arrows*) and bacterial (*black arrows*) cells. **c** Optical image of *Gloeocapsa*-type colonies separated by a cyanobacterial filamentous matrix. **d** CSLM image of coccoid cyanobacteria colonies associated to a filamentous cyanobacteria matrix. **e**–**h** Optical images of black *Nostoc* and (**e**) and cf. *Gloeocapsa* (**f**) colonies and *Tychonema*-type (**g**) and *Plectonema*-type filaments (**h**). **i** CSLM image of a *Nostoc* colony

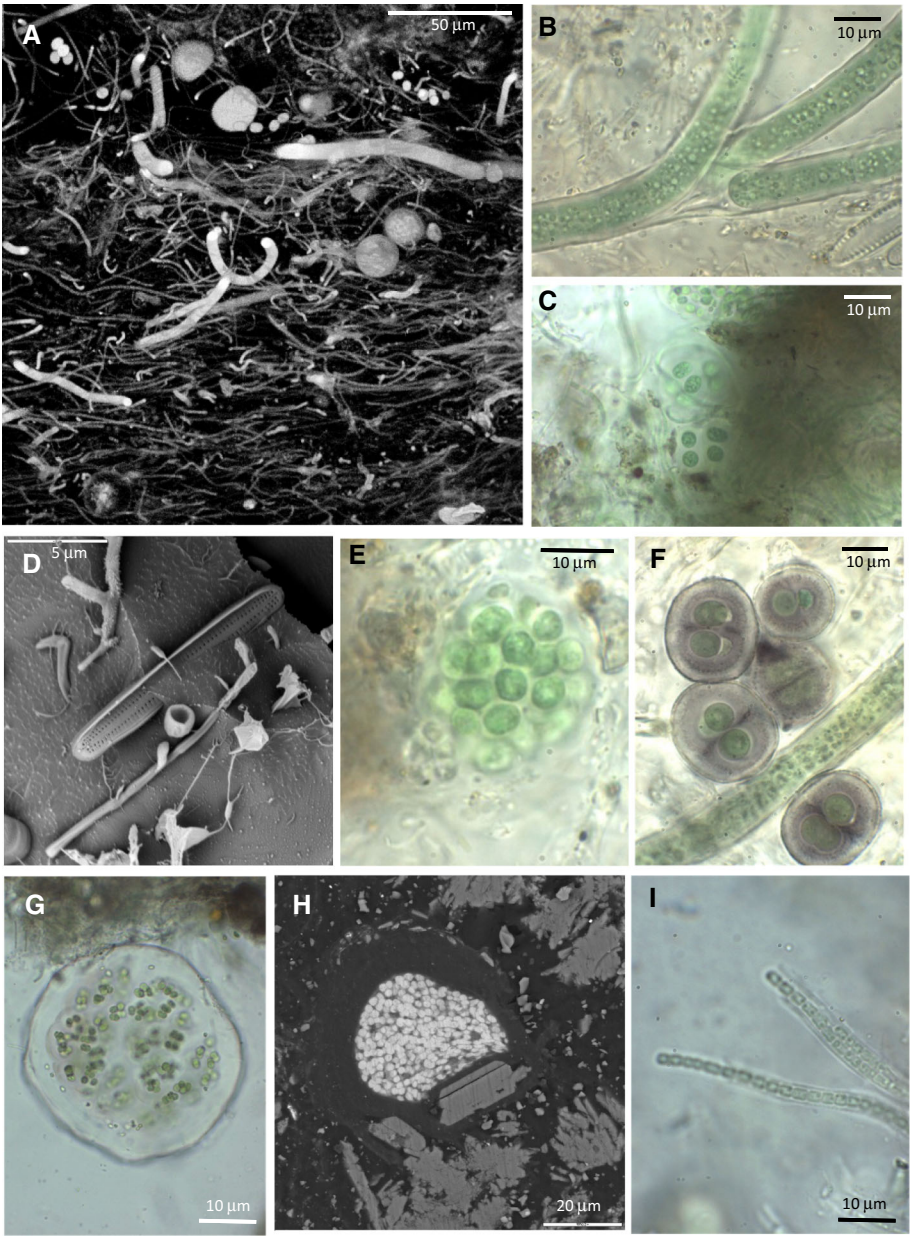

Fig. 8 Bottom layer of *pink* mat in stream C1. **a** CSLM image of the filamentous cyanobacteria matrix containing thick and thin cyanobacterial filaments. **b** Optical image of *Tolypothrix*-type showing the single false branching. **c** Optical image of colonies of *Gloeocapsa*-type cyanobacteria with no colour. **d** LTSEM image of a diatom frustule. **e–g** Optical images of cf. *Gloeocapsa* (**e**) cf. *Chroococcus* (**f**) and cf. *Aphanocapsa* (**g**) colonies. **h** SEM–BSE image of an cf. *Aphanothece* colony. **i** Optical image of *Pseudanabaena*-type filaments

The bottom layer of this mat type had a higher density of EPS and abundant mineral particles that were homogenously distributed through this layer (Fig. 6). The biological components in both layers were apparently similar.

The black surface colonies included old, non-fluorescent *Dichothrix* sp. colonies surrounded by fluorescent, medium size filaments, and larger spherical colonies made up of *Gloeocapsa* sp. with 1.5–1.7 μm diameter cells (Fig. 7c). These latter colonies were each separated and surrounded by cyanobacterial filaments of at least three different diameters: 1, 1.3 μm and a *Pseudanabaena*-type of 1.15 × 4 μm (Fig. 7c, d). Other genera present in this surface layer included *Chroococcus*-type (7.5 × 5.9 μm) with a thick sheath (10 × 7.3 μm); *Aphanocapsa*-type colonies of different cell sizes (3.7 and 5.4 μm); black *Nostoc* colonies with tightly arranged 6.5 μm diameter spherical cells (Fig. 7e); black *Gloeocapsa*-type colonies (Fig. 7f); and a *Tychonema*-type oscillatorian with thick bundles of 3.27 μm-wide, rigid filaments and large granules up to 3 × 2.6 μm in size, and some filaments terminating in a calyptra (arrow in Fig. 7g). The matrix also contained abundant populations of cf. *Plectonema*-with 1.9 × 3.2 μm granulated cells and a thick sheath (3.2–5.2 μm; Fig. 7h), narrow cyanobacterial filaments (0.7 μm in diameter) and a narrow (1 × 5 μm) *Pseudanabaena*-type cyanobacterium with aerotopes. *Nostoc* colonies, colonized by fungal-like hyphae (arrow in Fig. 7i) and thin cyanobacterial filaments, were also apparent by CLSM (Fig. 7i).

The bottom layer of the pink stream mat was composed of a large diversity of forms, with thick filaments, microcolonies and a matrix of fluorescent thin oscillatorians (Fig. 8a). Among the thick cyanobacteria, there were filaments of *Tolypothrix*-type (Fig. 8b) with

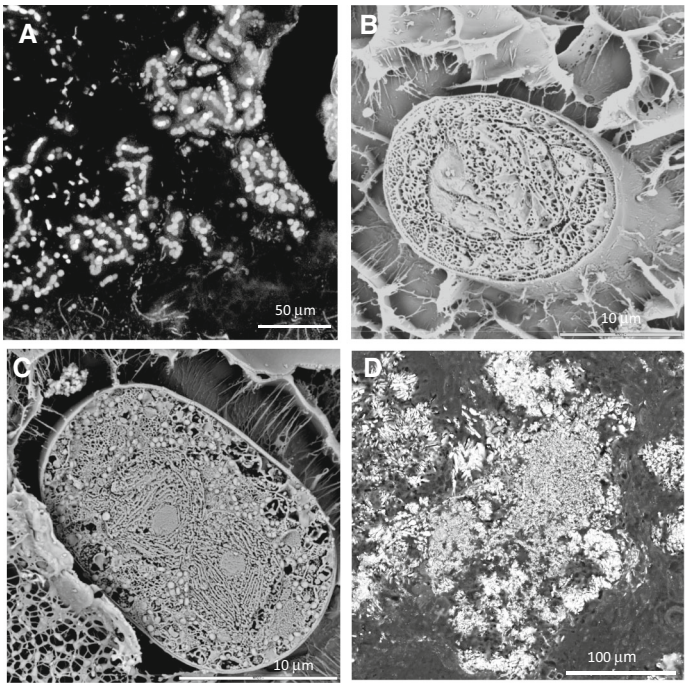

Fig. 9 Bottom layer of *pink* mat in stream C1. **a** CSLM image of *Nostoc* filaments. **b, c** LTSEM images of filamentous (**b**) and coccoid green algae (**c**). **d** SEM–BSE image of mineral particles with a low degree of cohesion embedded in the filamentous cyanobacteria matrix

8.4 × 8.9 μm cells and 7.7 × 6.4 μm heterocysts and *Tychonema*. As in the surface layer, there were associated colonies of *Gloeocapsa*-type cyanoabacteria with non-coloured sheaths (Fig. 8c), diatom frustules (Fig. 8d), violet *Gloeocapsa* cf. *compacta* in groups of 8 cells of 5.2 μm diameter (Fig. 8e), *Nostoc* colonies with tight 3.3 μm diameter spherical cells, and colonies of *Chroococcus*-type organisms (2.9 μm; Fig. 8f), *Aphanocapsa*-type (Fig. 8g) and *Aphanothece*-type cyanobacteria (Fig. 8h). The filamentous forms also included a 3.3 μm diameter cf. *Phormidium* with a curved end and cf. *Oscillatoria* with discoidal 5.4 × 1.45 μm cells. The thin filamentous cyanobacteria found at the surface were also present at the bottom layer, including abundant populations of *Pseudanabaena*-type (1.3 × 2.2; Fig. 8i), and a cf. *Leptolyngbya* of two cell sizes: 1.5 × 3.3 μm cells and 0.85 × 5.4 μm. *Nostoc* colonies and hormogonia (Fig. 9a), as well as cf. *Gloeothece* and cf. *Plectonema* were also observed, along with filamentous (Fig. 9b) and coccoid (Fig. 9c) green algae. Mineral particles were distributed among the cyanobacterial filaments and colonies as visualized by SEM–BSE (Fig. 9d).

Black mat in stream C1

The dark coloured mat from wet but not immersed parts of the stream did not show a clear stratified organization, but by SEM–BSE a thin surface layer with few mineral particles is detected (noted by arrows in Fig. 10a). The mat was a hard, brittle crust formed by a continuous layer of black microcolonies of different size (Fig. 10b) embedded in a mucilaginous pink-orange matrix. The bottom of the mat was pale green and mucilaginous, with numerous mineral particles (Fig. 10a) and dark green colonies.

The black surface colonies were composed of *Gloeocapsa*-type cyanobacteria, with variable cell sizes, ranging from 4 to 9 μm diameter (Fig. 10c). There is a second colony type containing larger cells (9 × 7.1 μm diameter) with a distinctive surface pattern (Fig. 10d). Diatoms were abundant, but mostly as broken and empty frustules (Fig. 10e). Filamentous green algae were also evident. The filamentous cyanobacteria in this mat included a thin *Tychonema* with wide sheaths and many cellular inclusions (Fig. 10f); *Calothrix* (8.2 μm wide at the heterocyst, which was 4.5 μm long) in a yellow lamellated sheath (Fig. 10g); narrow filaments with long cells (1.3 × 7.5 μm); a wide (4.8 μm) sheath of cf. *Pseudanabaena* with aerotopes at the ends of the cells; and *Nostoc* colonies with 4.4 μm spherical cells and 5.1 × 4.7 μm heterocysts. A colonial green alga with small cells (2.7 μm diameter) was also present. The mucilaginous colonies at the bottom were made of *Nostoc* (cells 5.15 × 4.7 μm; Fig. 11a), and within the colonies there were thin (1 μm) branching fungal-like hyphae (arrows in Fig. 11a). The pink orange matrix was formed by thin oscillatorians with yellow sheaths, along with cf. *Tychonema* (3 μm), and a thin filamentous cyanobacterium, with cells 1.7 μm wide and 4.3–5.2 μm long, with aerotopes and a black sheath 4.9 μm wide (Fig. 11b). Several other sizes of oscillatorians were observed including of cell dimensions 1.0 × 5.7 and 1.3 × 5.3 μm (Fig. 11c). Darkly pigmented *Gloeocapsa* and *Nostoc* colonies were also observed distributed throughout the matrix by SEM–BSE (arrows in Fig. 11d) and along with filaments of *Tolypothrix-type*, *Calothrix* and cf. *Tychonema* and a filamentous, branching green alga (11 μm diameter). Mineral particles were common in the vicinity of the filamentous mucilaginous cyanobacteria; in some areas there were loose aggregates of calcium carbonate (asterisk in Fig. 11d), while more heterogeneous mineral deposits harbouring diatoms remains and other mineral particles were found in other parts (Fig. 11e).

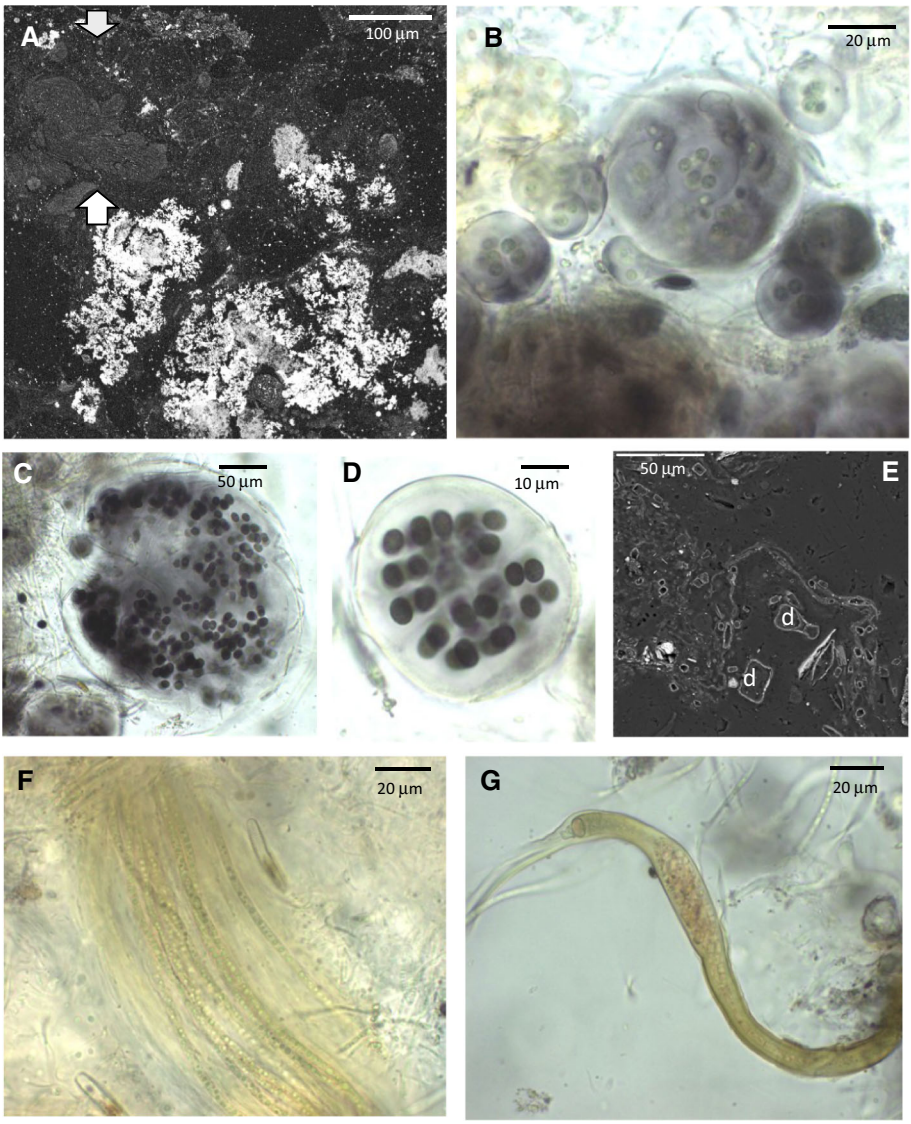

Fig. 10 Black mat in Stream C1. **a** General view of the upper part of the mat (SEM–BSE). *Arrows* note the upper layer without mineral precipitates. **b** Optical image of black cyanobacteria microcolonies of different size from the upper layer of the mat. **c**, **d**, optical images of *Gloecapsa*-type colonies. **e** SEM–BSE image of diatom frustules (**d**). **f**, **g** Optical images of cf. *Tychonema* (**f**) and *Calothrix* (**g**) filaments

Morphological diversity

Optical microscopy revealed 53 different cyanobacterial morphotypes (cellular arrangement and size) in the three microbial mats investigated (Table 2). Assuming that the different morphologies represented different taxa, Ward Hunt Lake mats and the C1 pink mats were more diverse in morphologies than the black mat community in which only 17

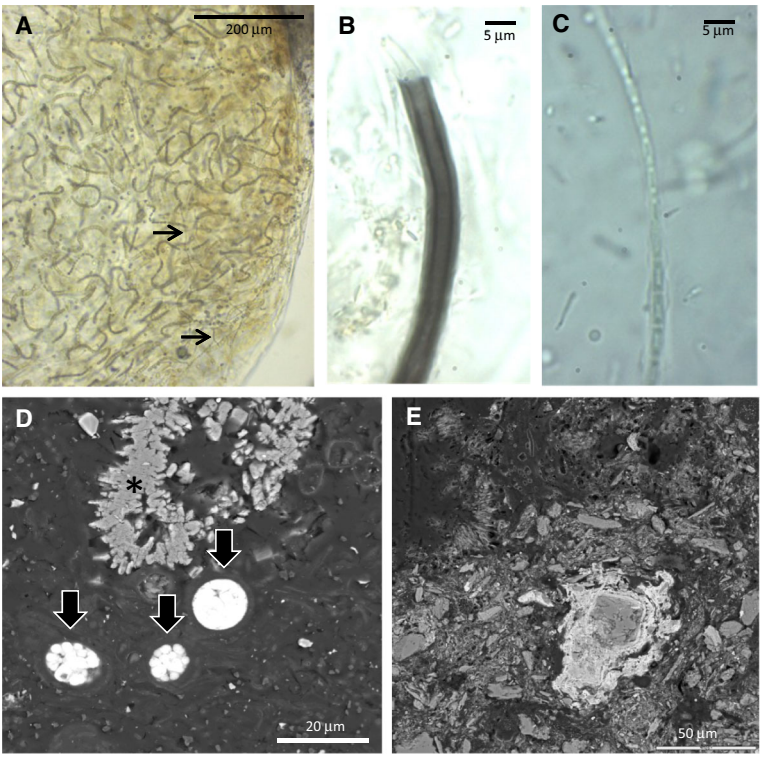

Fig. 11 Bottom layer of black mat in stream C1. **a** Optical image of *Nostoc* colony colonized by fungi (*arrows*). **b**, **c**, Optical images of thin filamentous cyanobacterium with black sheath (**b**) and *Pseudanabaena*-type filament (**c**). **d** SEM–BSE image of dark pigmented colonies (*arrows*) in the proximity of calcium carbonate particles (*asterisk*). **e** SEM–BSE image of heterogeneous mineral deposits

morphologies were distinguished. The most diverse group of cyanobacteria was *Pseudanabaena*-type with 10 different morphologies. Both cf-*Leptolyngbya* and *Nostoc* showed 8 different morphologies each. Only one morphospecies was present in the three microbial mats (cf. *Pseudanabaena* 1.1 × 4.6 µm) and 12 morphospecies distributed among the different genera were present in two out of the three mats. The oscillatorians found in the Ward Hunt and C1 pink mats (cf. *Leptolyngbya*, cf. *Plectonema*, cf. *Phormidium* and cf. *Oscillatoria*) were conspicuously absent from the black stream mat, which was especially rich and diverse in *Pseudanabaena*-type morphologies. *Dichothrix* was abundant in Ward Hunt Lake, with some decaying filaments of this genus in the pink mat. Some cyanobacterial genera were found predominantly in different habitats: Chroococcales cyanobacteria were remarkably more diverse and abundant in the mats from flowing water ecosystems, and *Gloeocapsa*-type was particularly diverse and abundant in this kind of ecosystems. The Oscillatoriales cf. *Tychonema* and the Nostocales genus *Tolypothrix* were also found only in mats from flowing water ecosystems, while *Dichothrix* was the most representative cyanobacterium in lake's microbial mats. *Nostoc* was well distributed in the three mats, but with diverse morphologies.

Table 2 Cyanobacterial morphological diversity of the three microbial mats investigated

Taxon	Ward Hunt Lake	Pink stream mat	Black stream mat
Pseudanabaena msp1 (1 × 5.75)			X
Pseudanabaena msp2 (1 × 8.9)			X
Pseudanabaena msp3 (1.1 × 4.6)	X	X	X
Pseudanabaena msp4 (1.3 × 3.4)	X		
Pseudanabaena msp5 (1.3 × 1.6–2)		X	
Pseudanabaena msp6 (1.3 × 7.5)			X
Pseudanabaena msp7 (1.3 × 5.3)			X
Pseudanabaena msp8 (1.5 × 2.7)	X		
Pseudanabaena msp9 (1.7 × 4.3) (black sheath)			X
Pseudanabaena msp10 (2 × 4.5)			X
Leptolyngbya msp1 (0.7 × 3.1)	X		
Leptolyngbya msp2 (0.8 × 4.8)	X		
Leptolyngbya msp3 (0.85 × 3.5)	X		
Leptolyngbya msp4 (0.85 × 5.4)		X	
Leptolyngbya msp5 (1 × 1.3)	X	X	
Leptolyngbya msp6 (1.2 × 2.9)	X	X	
Leptolyngbya msp7 (1.43 × 1.9)		X	
Leptolyngbya msp8 (1.55 × 3.4)	X		
Phormidium msp1 (2 × 4.1)	X		
Phormidium msp2 (3.3 × 2.6)		X	
Phormidium msp3 (4.6 × 10)	X		
Phormidium msp4 (6.9 × 9.2)	X		
Oscillatoria msp1 (5.4 × 1.45)		X	
Oscillatoria msp2 (10.7 × 5.2)	X		
Plectonema msp1 (1.5 × 2.4)	X	X	
Plectonema msp2 (1.9 × 3.2)		X	
Plectonema msp3 (2.1 × 2.2)	X		
Tychonema (3.27 × 3.1)		X	X
Aphanocapsa msp1 (2.5)	X		
Aphanocapsa msp2 (3.7)		X	
Aphanocapsa msp3 (5.4)		X	
Gloeocapsa msp1 (1.5–1.7)		X	
Gloeocapsa msp2 (2.6)	X	X	
Gloeocapsa msp3 (4)			X
Gloeocapsa msp4 (5.6 × 4.4)	X		X
Gloeocapsa msp5 (6.5 × 4.7)		X	X
Gloeocapsa msp6 (9)			X
Gloeothece		X	
Chroococcus msp1 (7.5 × 5.9)		X	
Chroococcus msp2 (2.9)		X	
Aphanothece msp1 (1.1 × 2.8) (refringent dot)		X	
Aphanothece msp2		X	
Dichothrix	X		

Table 2 continued

Taxon	Ward Hunt Lake	Pink stream mat	Black stream mat
Tolypothrix (8.4 × 8.9)		X	X
Calothrix			X
Nostoc msp1 3.3		X	
Nostoc msp2 (3.8 × 3.7)	X	X	
Nostoc msp3 (4.2 × 2.6)	X		
Nostoc msp5 (4.4)			X
Nostoc msp6 (5)	X		X
Nostoc msp7 (5.95 × 7.6)	X		X
Nostoc msp8 (6.5)		X	
Nostoc punctiforme		X	
Total taxa	23	26	17

The genera are given only by morphological similitude and does not have taxonomical value. The dimensions of the cells are in μm. 'msp' refers to morphospecies and may not have taxonomic value. When only one dimension is provided the cells are isodiametric

Discussion

Microbial mats are abundantly distributed in lakes, ponds and streams in both the polar regions (Vincent and Quesada 2012), but while they have received considerable attention in the Antarctic (Vincent et al. 1993; De los Ríos et al. 2004; Jungblut et al. 2005; Fernández-Valiente et al. 2007; Jungblut et al. 2010; Peeters et al. 2012; Hawes et al. 2013; Tytgat et al. 2014), much less is known about their composition and ecology in the Arctic (Bonilla et al. 2005; Jungblut et al. 2010; Varin et al. 2010, 2012; Lionard et al. 2012). Previous analyses of Arctic microbial mats have focused on their taxonomic and metabolic diversity, and the present study provides new insights into their morphotype composition and microstructural characteristics.

Our study identified 53 different cyanobacterial morphotypes in the three mats, including 23 in the Ward Hunt Lake mats, which is similar to the number of OTUs (24) obtained by molecular analyses of mats from the same shallow water site in Ward Hunt Lake (Jungblut et al. 2010). We found much higher morphotype diversity (26) in High Arctic stream mats than in the Jungblut et al. (2010) analysis of stream communities in the same northern Ellesmere Island region (16 OTUs). Phenotypic plasticity is well known in cyanobacteria, with the same organism having disparate morphologies under different environmental conditions (Loza et al. 2013). Our morphotype analysis may have therefore over-estimated diversity, although we were unable to differentiate coccoid forms such as *Synechococcus* that are known to be genetically diverse, including in High Arctic plankton communities (Van Hove et al. 2008). Thus, comparison between morphological and genetic diversity should be considered with caution.

There were large differences in morphotype composition among the three mat types sampled in the present study. In terms of genera, most mats described in the polar regions contain similar dominants (Jungblut et al. 2010; Varin et al. 2012), however our observations show that different morphospecies from the same genera can be present under different ecological conditions. The most striking differences were between the black mats occurring in intermittent flows and dominated by *Nostoc*, versus the pink stream mats

subject to continuous flowing water conditions in summer and dominated by oscillatorians. These two communities are similar to the black and orange mats occupying similar habitats in Antarctic desert streams (Vincent 1988) and it will be of great interest to compare these two communities in detail by metagenomic analysis, because this low resolution morphological study might not be adequate for community structure comparisons. Although sequencing of the 16S rRNA genes of High Arctic, alpine and Antarctic oscillatorians has indicated that genetically similar taxa are widely distributed throughout the cold biosphere, there is also increasing evidence of endemism among Antarctic cyanobacteria (Comte et al. 2007; Vyverman et al. 2010), and a pole-to-pole comparison of this analogous pair of polar desert stream mats could be especially informative.

The differences between the black and pink mats in the streams, and also relative to the Ward Hunt Lake mat, suggest that the community structure and microstructure, respond to environmental factors related to liquid water availability and habitat stability. These mats showed some structural similarities, with a dense, pigmented superficial layer with higher density of cells and a less cohesive bottom layer with higher accumulation of mineral precipitates. However, there were large differences in the distribution of biological and mineral components. The specific environmental factors of the different habitats, as well as the interactions and activities that occur within the mat (Tolker-Nielsen and Molin 2000; Glunk et al. 2011), likely determine this non-random microbial spatial distribution (Paerl and Pinckney 1996). For instance, the presence of highly pigmented cyanobacterial colonies in stream mats, could be related to the necessity of protection against direct exposure to solar UV and PAR radiation due to the temporality of the flows. In contrast, habitat stability may be a requisite for the *Dichothrix* film and its compact calcium carbonate precipitates in the Ward Hunt Lake mat.

Microbial components of cyanobacterial mats produce large amount of EPS generating an extracellular matrix where biological and biogeochemical interactions take place (Paerl and Pinckney 1996; Nichols et al. 2005). The EPS matrix also plays an important structural role in these microbial consortia (Dupraz et al. 2009; De los Ríos et al. 2014a). In Arctic microbial mats, cyanobacteria are the primary source of EPS genes (Varin et al. 2012), hence cyanobacterial EPS is the main structural component. This EPS matrix is not homogeneous, but rather exists as a series of microregions associated with the cyanobacterial colonies or trichomes (Decho 2000; De los Ríos et al. 2004). At the microscale level, the EPS creates relatively spacious pores that are likely to result in microbial microhabitats with their own distinctive chemical properties and assemblages of cells (Krembs et al. 2002). The mucilage also confers hydrophobicity to the mats that may aid their adhesion to the benthic substrate and reduce their tendency to be detached from the bottom by melting ice (Vézina and Vincent 1997). In addition, the EPS matrix play important roles in pH buffering, cryoprotection and resistance to desiccation for the microorganisms contained within (Vincent 1988; Krembs et al. 2002; De los Ríos et al. 2014b; De Maayer et al. 2014).

The different microenvironments within the polymeric matrix may support certain mineral transformations that are not chemically possible in the surrounding waters. Calcium carbonate precipitates occurred within these mats, generally in the proximity of cyanobacteria cells. They appeared to be more associated to EPS matrix rather than localized in or on the sheaths of cyanobacteria. Mineral precipitates identified as calcium carbonate are commonly found in many microbial mats (De los Ríos et al. 2004; Dupraz et al. 2009; Braissant et al. 2009; Glunk et al. 2011), and may be induced by metabolic activities (biologically-induced mineralization) or as result of environmentally driven mineralization of the organic matrix (biologically-influenced mineralization) (Dupraz et al.

2009). EPS contains negative charged functional groups that are known to chelate cations from the water column such as Ca^{2+} (Chan 2004; Braissant et al. 2007; Bontognali et al. 2010; Glunk et al. 2011). The degradation of EPS by heterotrophic metabolic reactions can favor the Ca^{2+} liberation and precipitation of calcium carbonate within the EPS matrix (Dupraz et al. 2004; Glunk et al. 2011). The observation of such particles in Arctic mats emphasizes the complex geomicrobiology of these highly structured microbial systems.

Acknowledgments We are grateful to PCPS for the logistic support to the High Arctic and Parks Canada for access to their facilities in Quttinirpaaq National Park. This project was funded by the Grants REN2000-0435, CGL2005-06549, POL2006-06635 and CTM2011-28736 from Spanish Ministry of Economy and Competitiveness, with funding of the microscopy studies through grants CTM2012-38222-C02-02 and CGL2013-42509. Additional support was provided by the Natural Sciences and Engineering Research Council of Canada and the Canada Research Chair program. The authors would like to thank to ICA and the MNCN (CSIC) microscopy services staff for technical assistance.

References

Bonilla S, Villeneuve V, Vincent WF (2005) Benthic and planktonic algal communities in a high arctic lake: pigment structure and contrasting responses to nutrient enrichment. J Phycol 41:1120–1130

Bontognali TRR, Vasconcelos C, Warthmann RJ, Bernasconi SM, Dupraz C, Strohmenger CJ, McKenzie J (2010) Dolomite formation within microbial mats in the coastal sabkha of Abu Dhabi (United Arab Emirates). Sedimentology 57:824–844

Braissant O, Decho AW, Dupraz C, Glunk C, Przekop KM, Visscher PT (2007) Exopolymeric substances of sulfate-reducing bacteria: interactions with calcium at alkaline pH and implication for formation of carbonate minerals. Geobiology 5:401–411

Braissant O, Decho AW, Prezekop KM, Gallagher K, Glunk C, Dupraz C, Visscher P (2009) Characteristics and turnover of exopolymeric substances in a hypersaline microbial mat. FEMS Microbiol Ecol 67:293–307

Chan C (2004) Microbial polysaccharides template assembly of nanocrystal fibers. Science 303:1656–1658

Comte K, Sabacka M, Carre-Mlouka A, Elster J, Komarek J (2007) Relationships between the Arctic and Antarctic cyanobacteria: three *Phormidium*-like strains evaluated by a polyphasic approach. FEMS Microbiol Ecol 59:366–376

De los Ríos A, Ascaso C, Wierzchos J, Fernandez-Valiente E, Quesada A (2004) Microstructural characterization of cyanobacterial mats from the McMurdo Ice Shelf, Antarctica. Appl Environ Microbiol 70:569–580

De los Ríos A, Cary C, Cowan D (2014a) The spatial structures of hypolithic communities in the Dry Valleys of East Antarctica. Polar Biol 37:1823–1833

De los Ríos A, Wierzchos J, Ascaso C (2014b) The lithic microbial ecosystems of Antarctica's McMurdo dry valleys. Antarct Sci 26:459–477

De Maayer P, Anderson D, Cary C, Cowan DA (2014) Some like it cold: understanding the survival strategies of psychrophiles. EMBO Rep 15:508–517

Decho AW (2000) Exopolymer microdomains as a structuring agent for heterogeneity within microbial biofilms. In: Riding RE, Awramik SM (eds) Exopolymer microdomains as a structuring agent for heterogeneity within microbial biofilms. Springer, Berlin, pp 9–15

Dupraz C, Visscher PT, Baumgartner LK, Reid RP (2004) Microbe-mineral interactions: early carbonate precipitation in a hypersaline lake (Eleuthera Island, Bahamas). Sedimentology 51:745–765

Dupraz C, Reid R, Braissant O, Decho AW, Norman RS, Visscher P (2009) Processes of carbonate precipitation in modern microbial mats. Earth Sci Rev 96:141–162

Fernández-Valiente E, Camacho A, Rochera C, Rico E, Vincent WF, Quesada A (2007) Community structure and physiological characterization of microbial mats in Byers Peninsula, Livingston Island (South Shetland Islands, Antarctica). FEMS Microbiol Ecol 59:377–385

Glunk C, Dupraz C, Braissant O, Gallagher K, Verrecchia E, Visscher P (2011) Microbially mediated carbonate precipitation in a hypersaline lake, Big Pond (Eleuthera, Bahamas). Sedimentology 58:720–738

Hawes I, Sumner D, Andersen D, Jungblut A, Mackey T (2013) Timescales of growth response of microbial mats to environmental change in an ice-covered Antarctic lake. Biology 2:151–176

Jungblut AD, Hawes I, Mountfort D, Hitzfeld B, Dietrich DR, Burns BP, Neilan BA (2005) Diversity within cyanobacterial mat communities in variable salinity meltwater ponds of McMurdo Ice Shelf, Antarctica. Environ Microbiol 7:519–529

Jungblut AD, Lovejoy C, Vincent WF (2010) Global distribution of cyanobacterial ecotypes in the cold biosphere. ISME J 4:191–202

Komárek J, Anagnostidis K (1989) Modern approach to the classification system of Cyanophytes, 4–Nostocales. Arch Hydrobiol Suppl. 82/Algol Stud 56:247–345

Komárek J, Anagnostidis, K. (1999) Cyanoprokaryota. 1. Chroococcales. In: Ettl H, Gärtner G, Heynig H, Mollenhauer D (eds) Süßwasserflora von Mitteleuropa. Begründet von A. Pascher. Band 19/1. Spektrum, Akademischer Verlag, Heidelberg, pp 1–548

Komárek J, Anagnostidis K (2005) Cyanoprokaryota. 2. Teil: Oscillatoriales. In: Büdel B, Gärdner G, Krienitz L, Schagerl M. (eds) Süsswasserflora von Mitteleuropa, vol. 19/2. Elsevier, München

Krembs C, Eicken H, Junge K, Deming JW (2002) High concentrations of exopolymeric substances in Arctic winter sea ice: implications for the polar ocean carbon cycle and cryoprotection of diatoms. Deep Sea Res Part I 49:2163–2181

Lionard M, Péquin B, Lovejoy C, Vincent WF (2012) Benthic cyanobacterial mats in the High Arctic: multi-layer structure and fluorescence responses to osmotic stress. Front Microbiol 3:140

Loza V, Perona E, Carmona J, Mateo P (2013) Phenotypic and genotypic characteristics of *Phormidium*-like cyanobacteria inhabiting microbial mats are correlated with the trophic status of running water. Eur J Phycol 48:235–252

Nichols C, Guezennec J, Bowman J (2005) Bacterial exopolysaccharides from extreme marine environments with special consideration of the southern ocean, sea ice, and deep-sea hydrothermal vents: a review. Mar Biotechnol 7:253–271

Noffke N, Gerdes G, Klenke T (2003) Benthic cyanobacteria and their influence on the sedimentary dynamics of peritidal depositional systems (siliciclastic, evaporitic salty, and evaporitic carbonatic). Earth Sci Rev 62:163–176

Paerl HW, Pinckney JL (1996) A mini-review of microbial consortia: their roles in aquatic production and biogeochemical cycling. Microb Ecol 31:225–247

Peeters K, Verleyen E, Hodgson D, Convey P, Ertz D, Vyverman W, Willems A (2012) Heterotrophic bacterial diversity in aquatic microbial mat communities from Antarctica. Polar Biol 35:543–554

Petroff AP, Sim MS, Maslov A, Krupenin M, Rothman DH, Bosak T (2010) Biophysical basis for the geometry of conical stromatolites. Proc Nat Acad Sci 107:9956–9961

Quesada A, Vincent WF (2012) Cyanobacteria in the cryosphere: snow, ice and extreme cold. In: Whitton BA (ed) Ecology of Cyanobacteria II. Springer, New York, pp 387–399

Quesada A, Vincent WF, Lean DRS (1999) Community and pigment structure of arctic cyanobacterial assemblages: the occurrence and distribution of UV-absorbing compounds. FEMS Microb Ecol 28:315–323

Quesada A, Sanchez-Contreras M, Fernández-Valiente E (2001) Tolerance of Antarctic cyanobacterial microbial mats to natural UV radiation. Nova Hedwigia 123:275–290

Singh SM, Elster J (2007) Cyanobacteria in Antarctic lake environments: a mini-review. In: Seckbach J (ed) Algae and cyanobacteria in extreme environments. Springer, Dordrecht, pp 303–320

Taton A, Hoffmann L, Wilmotte A (2008) Cyanobacteria in microbial mats of Antarctic lakes (East Antarctica)—a microscopical approach. Algol Stud 126:173–208

Tolker-Nielsen T, Molin S (2000) Spatial organization of microbial biofilm communities. Microb Ecol 40:75–84

Tytgat B, Verleyen E, Obbels D, Peeters K, De Wever A, D'hondt S, De Meyer T, Van Criekinge W, Vyverman W, Willems A (2014) Bacterial diversity assessment in Antarctic terrestrial and aquatic microbial mats: a comparison between bidirectional pyrosequencing and cultivation. PLoS One 9:e97564. doi:10.91371/journal.pone.0097564

Van Hove P, Vincent WF, Galand PE, Wilmotte A (2008) Abundance and diversity of picocyanobacteria in high arctic lakes and fjords. Algo Stud 126:209–227

Varin T, Lovejoy C, Jungblut A, Vincent WF, Corbeil J (2010) Metagenomic profiling of Arctic microbial mat communities as nutrient scavenging and recycling systems. Limnol Oceanogr 55:1901–1911

Varin T, Lovejoy C, Jungblut A, Vincent WF, Corbeil J (2012) Metagenomic analysis of stress genes in microbial mat communities from Antarctica and the High Arctic. Appl Environ Microbiol 78:549–559

Verleyen E, Sabbe K, Hodgson DA, Grubisic S, Taton A, Cousin S, Wilmotte A, De Wever A, Van Der Gucht K, Vyverman W (2010) Structuring effects of climate-related environmental factors on Antarctic microbial mat communities. Aquat Microb Ecol 59:11–24

Vézina S, Vincent WF (1997) Arctic cyanobacteria and limnological properties of their environment: Bylot Island, Nothwest Territories, Canada (73°N, 80°W). Polar Biol 17:523–534

Villeneuve V, Vincent WF, Komárek J (2001) Community structure and microhabitat characteristics of cyanobacterial mats in an extreme high Arctic environment: Ward Hunt Lake. Nova Hedwigia 123:199–224

Vincent WF (1988) Microbial ecosystems of Antarctica. Cambridge University Press, Cambridge

Vincent WF, Quesada A (2012) Cyanobacteria in high latitude lakes, rivers and seas. In: Whitton BA (ed) Ecology of Cyanobacteria II. Springer, New York, pp 371–385

Vincent WF, Castenholz RW, Downes MT, Howard-Williams C (1993) Antarctic cyanobacteria: light, nutrients, and photosynthesis in the microbial mat environment. J Phycol 29:745–755

Vincent WF, Gibson JAE, Pienitz R, Villenueve V (2000) Ice shelf microbial ecosystems in the High Arctic and implications for life on snowball Earth. Naturwissenschaften 87:137–141

Vyverman W, Verleyen E, Wilmotte A, Hodgson D, Willems A, Peeters K, Van de Vijver B, De Wever A, Leliaert F, Sabbe K (2010) Evidence for widespread endemism among Antarctic micro-organisms. Polar Sci 4:103–113